New Lanthanide Selenophosphates. Influence of Flux Composition on the Distribution of $[PSe_4]^{3-}/[P_2Se_6]^{4-}$ Units and the Stabilization of the Low-Dimensional Compounds $A_3REP_2Se_8$, and $A_2(RE)P_2Se_7$ (A = Rb, Cs; RE = Ce, Gd)

Konstantinos Chondroudis and Mercouri G. Kanatzidis*

Department of Chemistry, Michigan State University, East Lansing, Michigan 48824

Received January 8, 1998

The reaction of Ce or Gd with a molten mixture of $A_2Se/P_2Se_5/Se$ (A = Rb, Cs) produced the quaternary compounds $Rb_3CeP_2Se_8$ (**I**) and $Cs_3GdP_2Se_8$ (**II**), as well as $Rb_2CeP_2Se_7$ (**III**) and $Rb_2GdP_2Se_7$ (**IV**). The orange crystals of **I**, **II** and the red crystals of **III**, **IV** are air- and water-sensitive. Compounds **I**, **II** crystallize in the monoclinic space group $P2_1/c$, and for **I**, $a = 9.6013(2)$ Å, $b = 18.0604(1)$ Å, $c = 10.0931(1)$ Å, $\beta = 90.619(1)°$, and $Z = 4$. Compounds **III**, **IV** crystallize in the monoclinic space group $P2_1/n$, and for **IV**, $a = 10.137(2)$ Å, $b = 7.212(1)$ Å, $c = 20.299(2)$ Å, $\beta = 98.23(1)°$, and $Z = 4$. Compounds **I**, **II** have a 1-D structure with $[(RE)P_2Se_8]_n^{3n-}$ chains separated by A^+ cations. The RE^{3+} lanthanide cation is in a bicapped trigonal prismatic coordination with four tridentate $[PSe_4]^{3-}$ ligands. Compounds **III**, **IV** possess a 2-D structure. Each layer consists of $[RE(PSe_4)]_x$ "chains" interstitched in two dimensions by hexadentate $[P_2Se_6]^{4-}$ ligands. The trivalent RE cation is in a square antiprismatic coordination. The compounds were characterized with differential thermal analysis, far-IR, and solid-state UV/vis diffuse reflectance spectroscopy. Magnetic measurements indicate that the compounds obey the Curie law with μ_{eff} values close to those of the free RE^{3+} ions.

Introduction

The best experimental approach for the synthesis of new quaternary chalcophosphate compounds appears to be the polychalcophosphate molten salt method.[1] In the presence of metal ions these reactive fluxes give rise to highly anionic $[P_yQ_z]^{n-}$ units (Q = S, Se), which behave as ligands binding to the metal ions, forming new compounds. In the area of lanthanide/actinide chemistry, the high oxophilicity of the metals precludes the use of other low-temperature synthetic methods such as hydrothermal techniques, whereas the molten polychalcogenide approach offers the advantage of providing an oxygen-free, yet solvent-like, environment. As a result, the application of this technique into the f-block metal chemistry was met with spectacular success, yielding some very unusual compounds such as $K_4Eu(PSe_4)_2$,[2a] $KEuPSe_4$,[2b] $K_2UP_3Se_9$,[3a] $Rb_4U_4P_4Se_{26}$,[3b] and the $K(RE)P_2Se_6$ (RE = Y, La, Ce, Pr, Gd) series.[4] To obtain a better picture of the lanthanide chemistry, we continued this work, since a wide compositional range remains unexplored. By employing the fluxes, this can be accomplished in a systematic way, since by adjusting the flux composition we can affect the presence and distribution of the various $[P_yQ_z]^{n-}$ units in the reaction medium and eventually in the final product.[5] We have already reported on the compound $Rb_9Ce(PSe_4)_4$, which contains discrete $[Ce(PSe_4)_4]^{9-}$ anions,[6] and here we report the synthesis, structural characterization, and optical and thermal properties of $Rb_3CeP_2Se_8$ (**I**), $Cs_3GdP_2Se_8$ (**II**), $Rb_2CeP_2Se_7$ (**III**), and $Rb_2GdP_2Se_7$ (**IV**), which adopt new structure types.

Experimental Section

Reagents. The reagents mentioned in this study were used as obtained unless noted otherwise: (i) Ce and Gd metal (99.99%) were acquired from Johnson Matthey/AESAR Group, Seabrook, NH; (ii) red phosphorus powder, Morton Thiokol, Inc., −100 mesh, Danvers, MA; (iii) rubidium and cesium metal, analytical reagents, Johnson Matthey/AESAR; (iv) selenium powder, 99.5+% purity, −100 mesh, Aldrich Chemical Co., Inc., Milwaukee, WI; (v) *N*,*N*-dimethylformamide (DMF) reagent grade, EM Science, Inc., Gibbstown, NJ; (vi) diethyl ether, ACS anhydrous, EM Science.

Syntheses. A_2Se (A = Rb, Cs) were prepared by reacting stoichiometric amounts of the elements in liquid ammonia as described elsewhere.[7]

P_2Se_5. The amorphous phosphorus selenide glass "P_2Se_5" was prepared by heating a stoichiometric ratio of the elements as described elsewhere.[7]

Preparation of $Rb_3CeP_2Se_8$ (I). (a) Single crystals of **I** were synthesized from a mixture of Ce (0.6 mmol), P_2Se_5 (0.6 mmol), Rb_2Se (1.2 mmol), and Se (3.0 mmol), which was sealed under vacuum in a Pyrex tube and heated to 500 °C for 4 days, followed by cooling to 150 °C at 3 °C h^{-1}. The excess $Rb_xP_ySe_z$ flux was removed by washing with DMF to reveal a mixture of red polyhedral plates of $Rb_3CeP_2Se_8$ (60%) and orange rodlike crystals of $Rb_9Ce(PSe_4)_4$ (40%).[6] The $Rb_3CeP_2Se_8$ crystals decompose on exposure to air (2−3 h) and water (1 min). (b) Pure material was synthesized from a mixture of Ce (0.40 mmol), P (0.80 mmol), Rb_2Se (0.60 mmol), and Se (2.60 mmol) heated to 570 °C for 2 days followed by cooling to 150 °C at 24 °C h^{-1}. Small amounts of $Rb_xP_ySe_z$ flux and $Rb_9Ce(PSe_4)_4$ were removed by washing the material with a mixture of DMF/H_2O (30:1) for 2 min.

(1) Kanatzidis, M. G. *Curr. Opin. Solid State Mater. Sci.* **1997**, *2*, 139.
(2) (a) Chondroudis, K.; McCarthy, T. J.; Kanatzidis, M. G. *Inorg. Chem.* **1996**, *35*, 840. (b) Chondroudis, K.; Kanatzidis, M. G. To be published.
(3) (a) Chondroudis, K.; Kanatzidis, M. G. *C. R. Acad. Sci. Paris, Ser. II: Mec., Phys. Chim., Astron.* **1996**, *322*, 887. (b) Chondroudis, K.; Kanatzidis, M. G. *J. Am. Chem. Soc.* **1997**, *119*, 2574.
(4) (a) Chen, J. H.; Dorhout, P. K. Ostenson, J. E. *Inorg. Chem.* **1996**, *35*, 5627. (b) Chen, J. H.; Dorhout, P. K. *Inorg. Chem.* **1995**, *34*, 5705.
(5) Chondroudis, K.; Hanko, J. A.; Kanatzidis, M. G. *Inorg. Chem.* **1997**, *36*, 2623.
(6) Chondroudis, K.; Kanatzidis, M. G. *Inorg. Chem. Commun.* **1998**, *1*, 55.
(7) McCarthy, T. J.; Kanatzidis, M. G. *Inorg. Chem.* **1995**, *34*, 1257.

S0020-1669(98)00025-1 CCC: $15.00
Published on Web 07/10/1998

Table 1. Crystallographic Data for $Rb_3CeP_2Se_8$ (**I**) and $Cs_2GdP_2Se_7$ (**IV**)

formula	$Rb_3CeP_2Se_8$	$Cs_2GdP_2Se_7$	formula	$Rb_3CeP_2Se_8$	$Cs_2GdP_2Se_7$
fw	1090.15	1037.73	Z	4	4
space group	$P2_1/c$ (No. 14)	$P2_1/n$ (No. 14)	λ(Mo Kα), Å	0.71069	0.71069
a, Å	9.6013(2)	10.137(2)	D_{calc}, g/cm^3	4.137	4.692
b, Å	18.0604(1)	7.212(1)	μ, cm^{-1}	276.66	269.36
c, Å	10.0931(1)	20.299(2)	temp, °C	−100	25
β, deg	90.619(1)	98.23(1)	final R/R_w,[a] %	3.0/3.3	3.1/2.6
V, Å^3	1750.07(3)	1468.8(4)			

[a] $R = \sum(|F_o| - |F_c|)/\sum|F_o|$, $R_w = \{\sum_w(|F_o| - |F_c|)^2/\sum_w|F_o|^2\}^{1/2}$. The reflections were weighted according to $w = 1/[\sigma(F_o^2)^2 + (0.03F_o^2)^2]^{1/2}$ (where w = weight of a given F_o).

Further washing with ether revealed pure red-orange microcrystals of $Rb_3CeP_2Se_8$ (86%). Microprobe analysis gave a composition of $Rb_{3.2}Ce_{1.0}P_{2.2}Se_{7.9}$.

Preparation of $Cs_3GdP_2Se_8$ (II). A mixture of Gd (0.40 mmol), P (0.80 mmol), Cs_2Se (0.60 mmol), and Se (2.60 mmol) was heated to 570 °C for 2 days followed by cooling to 150 °C at 24 °C h^{-1}. Small amounts of $Cs_xP_ySe_z$ flux were removed by washing the material with a mixture of DMF/H_2O (30:1) for 2 min. Further washing with ether revealed pure yellow microcrystals of $Cs_3GdP_2Se_8$ (84%). The crystals decompose on exposure to air (2−3 h) and water (1 min). Microprobe analysis gave a composition of $Cs_{2.8}Gd_{1.0}P_{2.1}Se_{8.1}$.

Preparation of $Rb_2CeP_2Se_7$ (III). A mixture of Ce (0.40 mmol), P (0.80 mmol), Rb_2Se (0.40 mmol), and Se (2.40 mmol) was heated to 650 °C for 2 days followed by cooling to 150 °C at 25 °C h^{-1}. Small amounts of $Rb_xP_ySe_z$ flux were removed by washing with DMF. Further washing with ether revealed pure red microcrystals of $Rb_2CeP_2Se_7$ (81%). The crystals decompose on exposure to air (3−5 h) and water (3 min). Microprobe analysis gave a composition of $Rb_{1.9}Ce_{1.0}P_{2.3}Se_{7.3}$.

Preparation of $Cs_2GdP_2Se_7$ (IV). (a) Single crystals of **IV** were synthesized from a mixture of Gd (0.6 mmol), P_2Se_5 (0.6 mmol), Cs_2Se (0.6 mmol), and Se (3.0 mmol), which was sealed under vacuum in a Pyrex tube and heated to 515 °C for 4 days followed by cooling to 150 °C at 3 °C h^{-1}. Most of the $Cs_xP_ySe_z$ flux was removed by washing with DMF to reveal a mixture of small orange plates of $Cs_2GdP_2Se_7$ (40%) and black powder of residual flux (60%). The $Cs_2GdP_2Se_7$ crystals decompose on exposure to air (3−5 h) and water (3 min). (b) Pure material was synthesized from a mixture of Gd (0.40 mmol), P (0.80 mmol), Cs_2Se (0.40 mmol), and Se (2.40 mmol) heated to 650 °C for 2 days followed by cooling to 150 °C at 24 °C h^{-1}. Small amounts of $Cs_xP_ySe_z$ flux were removed by washing with DMF. Further washing with ether revealed pure red-orange microcrystals of $Cs_2GdP_2Se_7$ (87%). Microprobe analysis gave a composition of $Cs_{1.8}Gd_{1.0}P_{2.1}Se_{7.3}$.

Physical Measurements. Powder X-ray Diffraction. Analyses were performed using a calibrated Rigaku-Denki/RW400F2 (Rotaflex) rotating anode powder diffractometer controlled by an IBM computer, operating at 45 kV/100 mA and with a 1°/min scan rate, employing Ni-filtered Cu radiation. Powder patterns were calculated with the CERIUS^2 software.[8] Calculated and observed XRD patterns are deposited with the Supporting Information.

Infrared Spectroscopy. Infrared spectra, in the far-IR region (50−600 cm^{-1}), were recorded on a computer controlled Nicolet 750 Magna-IR Series II spectrophotometer equipped with a TGS/PE detector and silicon beam splitter in 4 cm^{-1} resolution. The samples were ground with dry CsI into a fine powder and pressed into translucent pellets.

Solid-State UV/Vis/Near-IR Spectroscopy. Optical diffuse reflectance measurements were performed as described elsewere.[5]

Differential Thermal Analysis. Differential thermal analysis (DTA) experiments were performed on a computer-controlled Shimadzu DTA-50 thermal analyzer. Typically a sample (∼25 mg) of ground crystalline material was sealed in quartz ampules under vacuum. A quartz ampule of equal mass filled with Al_2O_3 was sealed and placed on the reference side of the detector. The samples were heated to the desired temperature at 10 °C/min, then isothermed for 10 min, and finally cooled to 50 °C at the same rate. To evaluate congruent melting, we compared the X-ray powder diffraction patterns before and after the DTA experiments. The stability/reproducibility of the samples were monitored by running multiple heating/cooling cycles.

Semiquantitative Microprobe Analyses. The analyses were performed using a JEOL JSM-6400V scanning electron microscope (SEM) equipped with a TN 5500 EDS detector. Data acquisition was performed with an accelerating voltage of 20 kV and 30 s accumulation time.

Magnetic Susceptibility Measurements. The magnetic response of the compounds was measured over the range of 5−300 K using a MPMS Quantum Design SQUID magnetometer. Samples were ground to a fine powder to minimize possible anisotropic effects and loaded into PVC containers. Corrections for the diamagnetism of the PVC sample container were made by measuring the magnetic response of the empty container under identical conditions. Corrections for core atom diamagnetism were also applied.

Single-Crystal X-ray Crystallography. A Siemens SMART Platform CCD diffractometer was used to collect data from a crystal of **I**. An empirical absorption correction (SADABS)[9] was applied to the data. Intensity data for **IV** were collected using a Rigaku AFC6S four-circle automated diffractometer equipped with a graphite crystal monochromator. An empirical absorption correction based on ψ scans was applied during initial stages of refinement. The space groups were determined from systematic absences and intensity. No crystal decay was detected in any of the compounds. The structures were solved by direct methods using SHELXS-86 software[10a] (for all compounds), and full matrix least squares refinement was performed using the TEXSAN software package.[10b]

The data collection parameters for **I** and **IV** are given in Table 1. The coordinates of all atoms, average isotropic temperature factors, and their estimated standard deviations are given in Tables 2 and 3.

Results and Discussion

Description of Structures. $Rb_3CeP_2Se_8$ (**I**) and $Cs_3GdP_2Se_8$ (**II**) are isostructural, but since the single-crystal structure determination was performed on **I**, the discussion will refer mainly to this compound. A more descriptive formula for **I** is $Rb^+{}_3Ce^{3+}[(PSe_4)^{3-}]_2$. The structure contains infinite $[Ce(PSe_4)_2]_n^{3n-}$ chains separated by Rb^+ cations which propagate along the [100] direction; see Figure 1. The chains consist of Ce^{3+} cations linked by tridentate $[PSe_4]^{3-}$ ligands; see Figure 2A. Each Ce atom is coordinated by four such ligands to yield a coordination polyhedron of a bicapped trigonal prism; see Figure 2B. Each $[PSe_4]^{3-}$ ligand coordinates to two neighboring Ce centers, by employing one Se atom for every Ce, whereas a third Se atom acts as a bridge to both Ce centers. The fourth Se atom remains terminal. This structural motif has been observed in other chalcophosphates such as $KTiPSe_5$,[11] and K_2-

(8) *CERIUS*^{2}, Version 1.6; Molecular Simulations Inc.: Cambridge, England, 1994.
(9) Blessing, R. H. *Acta Crystallogr.* **1995**, *A51*, 33.
(10) (a) Sheldrick, G. M. In *Crystallographic Computing 3*; Sheldrick, G. M., Kruger, C., Goddard, R., Eds.; Oxford University Press: Oxford, England, 1985; p 175. (b) Gilmore G. J. *Appl. Crystallogr.* **1984**, *17*, 42.
(11) Chondroudis, K.; Kanatzidis, M. G. *Inorg. Chem.* **1995**, *34*, 5401.

Table 2. Positional Parameters and B_{eq}[a] for $Rb_3CeP_2Se_8$

atom	*x*	*y*	*z*	B_{eq},[a] Å^2
Ce	0.72784(5)	0.513 01(2)	0.026 30(5)	0.91(1)
Rb(1)	0.7631(1)	0.464 75(5)	0.482 86(9)	1.68(2)
Rb(2)	0.6097(1)	0.794 45(5)	0.133 2(1)	2.34(2)
Rb(3)	0.0975(1)	0.710 53(5)	0.141 5(1)	3.75(3)
Se(1)	1.0396(1)	0.522 76(4)	0.178 36(9)	1.11(2)
Se(2)	1.1719(1)	0.343 40(4)	0.091 20(8)	1.32(2)
Se(3)	1.0733(1)	0.375 53(5)	0.427 13(8)	1.35(2)
Se(4)	0.8120(1)	0.370 49(5)	0.167 63(9)	1.52(2)
Se(5)	0.5557(1)	0.515 39(5)	−0.254 20(8)	1.41(2)
Se(6)	0.3824(1)	0.682 64(5)	0.355 82(9)	1.45(2)
Se(7)	0.4677(1)	0.621 57(5)	0.024 60(8)	1.15(2)
Se(8)	0.7233(1)	0.613 69(5)	0.272 39(8)	1.29(2)
P(1)	0.9728(2)	0.597 9(1)	−0.222 1(2)	0.90(4)
P(2)	0.4982(2)	0.603 2(1)	0.240 3(2)	0.82(4)

[a] *B* values for anisotropically refined atoms are given in the form of the isotropic equivalent displacement parameter defined as $B_{eq} = (4/3)[a^2B(1,1) + b^2B(2,2) + c^2B(3,3) + ab(\cos\gamma)B(1,2) + ac(\cos\beta)B(1,3) + bc(\cos\alpha)B(2,3)]$.

Table 3. Positional Parameters and B_{eq}[a] for $Cs_2GdP_2Se_7$

atom	*x*	*y*	*z*	B_{eq},[a] Å^2
Gd	0.19034(5)	0.02248(8)	0.848 34(2)	1.15(1)
Cs(1)	−0.35622(7)	−0.0006(1)	0.797 78(4)	2.67(2)
Cs(2)	0.26145(7)	0.4983(1)	1.026 75(4)	2.32(2)
Se(1)	0.3082(1)	−0.0839(2)	0.724 20(5)	1.51(2)
Se(2)	0.0722(1)	−0.2560(2)	0.596 94(6)	1.43(2)
Se(3)	0.1044(1)	0.2367(2)	0.603 55(6)	1.59(2)
Se(4)	−0.02913(9)	−0.0016(2)	0.735 24(5)	1.65(2)
Se(5)	−0.0069(1)	−0.2402(2)	0.896 86(6)	1.48(2)
Se(6)	−0.0150(1)	0.2504(2)	0.899 24(6)	1.60(3)
Se(7)	0.2642(1)	0.0053(2)	1.019 24(5)	1.79(2)
P(1)	0.3852(2)	0.4828(4)	0.836 4(1)	1.17(5)
P(2)	0.0668(2)	0.0005(5)	1.048 5(1)	1.19(5)

[a] *B* values for anisotropically refined atoms are given in the form of the isotropic equivalent displacement parameter defined as $B_{eq} = (4/3)[a^2B(1,1) + b^2B(2,2) + c^2B(3,3) + ab(\cos\gamma)B(1,2) + ac(\cos\beta)B(1,3) + bc(\cos\alpha)B(2,3)]$.

MP_2S_7 (M = V, Cr).[12] The Ce polyhedra share edges along the direction of the chain, in such a way that there is an alternating short−long−short Ce−Ce distance in the chain. The long distance (e.g. Ce−Ce′) is 5.280(1) Å, whereas the short distance (e.g. Ce−Ce″) is 4.426(1) Å. The Ce−Se distances average at 3.15(4) Å and compare very well with those found in $Rb_9Ce(PSe_4)_4$.[6] The longest Ce−Se distances are exhibited by the capping Se atoms [Se(1′), Se(5)], Figure 2B. The P−Se distances range from 2.164(2) to 2.227(2) Å with the terminal selenium atoms displaying the shorter distances. The chains are separated by Rb^+ ions that are located in three different sites. Rb(1) is coordinated by eight Se atoms [range of Rb(1)−Se distances, 3.403(1)-3.898(1) Å; av 3.568 Å], Rb(2) is also eight-coordinate [3.438(1)−3.978(1) Å; av 3.654 Å], and Rb(3) is six-coordinate [3.457(1)−3.609(1) Å; av 3.529 Å]. Tables of selected distances and angles for $Rb_3CeP_2Se_8$ are given in Table 4.

$Rb_2CeP_2Se_7$ (**III**) and $Cs_2GdP_2Se_7$ (**IV**) are isostructural as well, and only the crystal structure of **IV** was determined. The compound is mixed ligand containing both $[PSe_4]^{3-}$ and $[P_2Se_6]^{4-}$ units. A more descriptive formula for **IV** is $(Cs^+)_4(Gd^{3+})_2[(PSe_4)^{3-}]_2(P_2Se_6)^{4-}$. The $[Gd_2(PSe_4)_2(P_2Se_6)]_n^{4n-}$ layers propagate along the [101] direction, and they are separated by Cs^+ cations; see Figure 3. The layers consist of infinite $[Gd(PSe_4)]_x$ "chains" parallel to the [010] direction. These

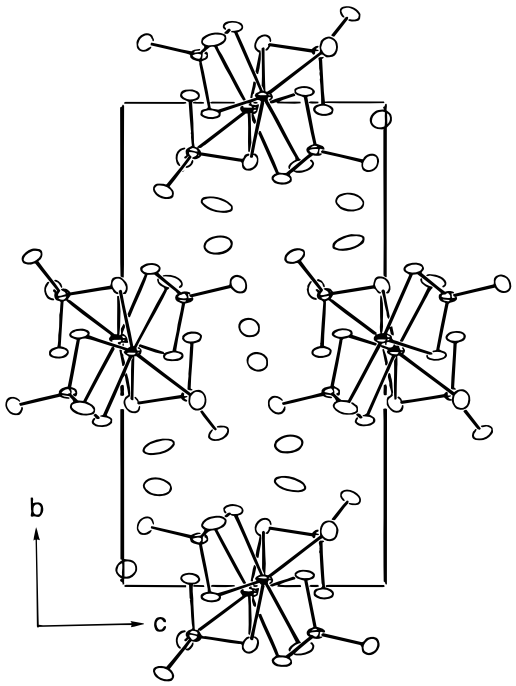

Figure 1. ORTEP representation of $Rb_3CeP_2Se_8$ as viewed down the *a*-axis (70% ellipsoids). In the infinite part of the structure Ce is shown as octant shaped ellipses, selenium as open ellipses, and phosphorus as crossed ellipses with no shading. Rb cations between the chains are shown as open ellipses.

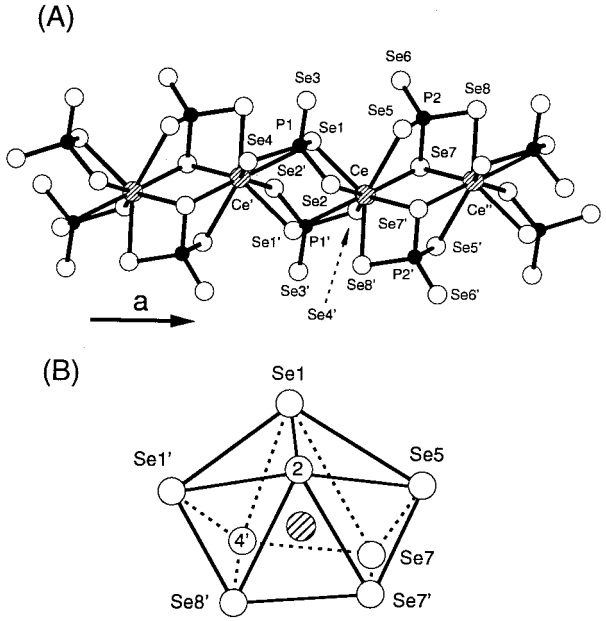

Figure 2. (A) View of a single $[CeP_2Se_8]_n^{3n-}$ chain with labeling. (B) Bicapped trigonal prismatic environment around Ce^{3+}.

chains are then connected into layers by hexadentate $[P_2Se_6]^{4-}$ units which coordinate to two Gd^{3+} centers in different chains employing all six Se atoms; see Figure 4A. There is a crystallographic center of symmetry located in the center of every P−P bond. Each tetradentate $[PSe_4]^{3-}$ unit bridges three Gd^{3+} centers in a unique mode of coodination. Furthermore, each Gd^{3+} center is coordinated by three $[PSe_4]^{3-}$ units. The Gd^{3+} coordination is completed by one $[P_2Se_6]^{4-}$ unit, yielding a square antiprismatic environment for the metal, Figure 4B. The Gd−Se distances average at 3.07(2) Å slightly shorter than Ce−Se as expected for the smaller Gd ion.[13] The P−Se

(12) Tremel, W.; Kleinke, H.; Derstroff, V.; Reisner, C. *J. Alloys Compd.* **1995**, *219*, 73.

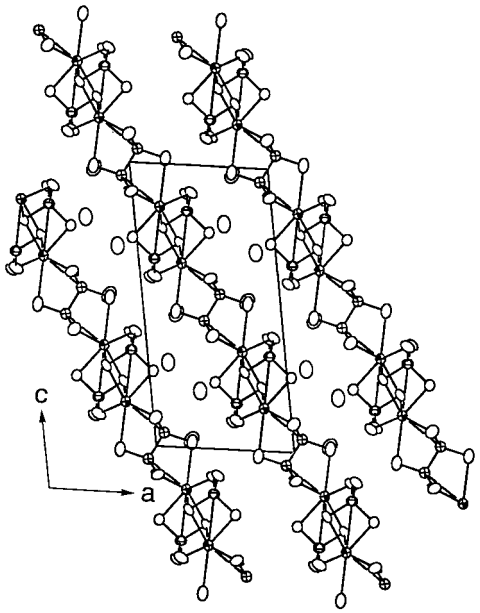

Figure 3. ORTEP representation of $Cs_2GdP_2Se_7$ as viewed down the *b*-axis. (80% ellipsoids). In the infinite part of the structure Gd is shown as octant shaped ellipses, selenium as open ellipses, and phosphorus as crossed ellipses with no shading. Cs cations between the layers are shown as open ellipses.

Table 4. Selected Distances (Å) and Angles (deg) for $Rb_3CeP_2Se_8$ with Estimated Standard Deviations in Parentheses

Ce−Se(1)	3.126(1)	P(1)−Se(1)	2.227(2)
Ce−Se(1′)	3.354(1)	P(1)−Se(2)	2.200(2)
Ce−Se(2)	3.014(1)	P(1)−Se(3)	2.165(2)
Ce−Se(4′)	3.048(1)	P(1)−Se(4)	2.207(2)
Ce−Se(5)	3.263(1)	P(2)−Se(5)	2.208(2)
Ce−Se(7)	3.111(1)	P(2)−Se(6)	2.164(2)
Ce−Se(7′)	3.175(1)	P(2)−Se(7)	2.218(2)
Ce−Se(8′)	3.079(1)	P(2)−Se(8)	2.190(2)
Ce−Ce′	5.280(1)		
Ce−Ce″	4.426(1)		

Se(1)−Ce−Se(1′)	70.90(3)	Ce−Se(1)−P(1)	88.23(7)
Se(1)−Ce−Se(2)	71.60(3)	Ce−Se(2)−P(1)	91.61(6)
Se(1)−Ce−Se(4′)	86.97(3)	Ce−Se(5)−P(2)	92.80(6)
Se(1)−Ce−Se(5)	77.77(3)	Ce−Se(7)−P(2)	96.78(6)
Se(1)−Ce−Se(7)	99.41(3)	Ce−Se(1)−Ce′	109.10(3)
Se(1)−Ce−Se(7′)	133.75(3)	Ce−Se(7)−Ce″	89.53(3)
Se(1′)−Ce−Se(5)	146.89(3)		
Se(1)−Se(1′)−Se(2)	53.70(2)	Se(1)−P(1)−Se(2)	108.5(1)
Se(1)−Se(4′)−Se(7)	77.00(3)	Se(1)−P(1)−Se(3)	113.31(9)
Se(1)−Se(2)−Se(7′)	104.85(3)	Se(1)−P(1)−Se(4)	104.82(9)
Se(1)−Se(2)−Se(8′)	98.45(3)	Se(5)−P(2)−Se(6)	119.1(1)
Se(2)−Se(7′)−Se(7)	90.09(3)	Se(5)−P(2)−Se(7)	100.32(9)
		Se(5)−P(2)−Se(8)	107.8(1)

distances range from 2.167(3) to 2.214(4) Å. The P−P bond is 2.224(7) Å. The layers are separated by Cs^+ ions that are located in two different sites. Cs(1) is coordinated by seven Se atoms [range of Cs(1)−Se distances, 3.565(2)−3.921(2) Å; av 3.751 Å], and Cs(2) is ten-coordinate [3.559(2)−3.982(2) Å; av 3.747 Å]. Tables of selected distances and angles for $Cs_2GdP_2Se_7$ are given in Table 5.

Synthesis, Spectroscopy, and Thermal Analysis

Chemical Considerations. The syntheses of these compounds involves the oxidation of the lanthanide metals and the reduction of the polyselenide ions in the $A_n[P_ySe_z]$ flux. The

(13) Shannon, R. D. *Acta Crystallogr.* **1976**, *A32*, 751.

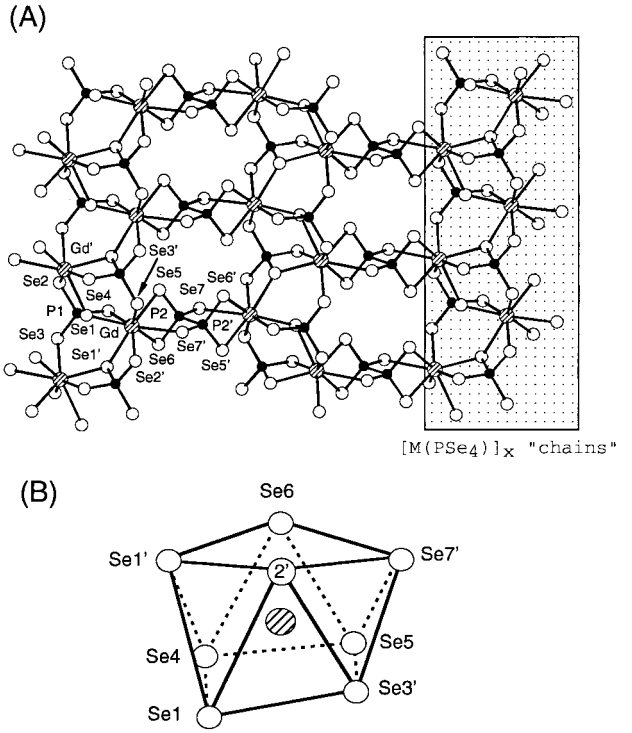

Figure 4. (A) Perpendicular view (along [101]) of a $[GdP_2Se_7]_n^{2n-}$ layer with labeling. (B) Square antiprismatic environment around Gd^{3+}.

Table 5. Selected Distances (Å) and Angles (deg) for $Cs_2GdP_2Se_7$ with Estimated Standard Deviations in Parentheses

Gd−Se(1)	3.038(1)	P(1)−Se(1)	2.214(4)
Gd−Se(1′)	3.199(2)	P(1)−Se(2)	2.194(4)
Gd−Se(2′)	2.969(2)	P(1)−Se(3)	2.194(4)
Gd−Se(3′)	2.991(2)	P(1)−Se(4)	2.205(3)
Gd−Se(4)	2.965(2)	P(2)−Se(5)	2.187(4)
Gd−Se(5)	3.020(2)	P(2)−Se(6)	2.199(4)
Gd−Se(6)	2.953(2)	P(2)−Se(7)	2.167(3)
Gd−Se(7′)	3.445(2)	P(2)−P(2′)	2.224(7)

Se(1)−Gd−Se(1′)	79.28(3)	Gd−Se(1)−P(1)	89.08(9)
Se(1)−Gd−Se(2′)	92.99(4)	Gd−Se(4)−P(1)	91.1(1)
Se(1)−Gd−Se(3′)	76.06(4)	Gd−Se(5)−P(2)	85.1(1)
Se(1)−Gd−Se(4)	71.55(4)	Gd−Se(6)−P(2)	86.6(1)
Se(1)−Gd−Se(5)	118.01(5)		
Se(1)−Gd−Se(6)	144.25(5)	Gd−Se(1)−Gd′	129.35(6)
Se(1)−Gd−Se(7′)	140.51(4)		
Se(1)−Se(4)−Se(5)	92.41(5)	Se(1)−P(1)−Se(2)	104.6(2)
Se(3′)−Se(1)−Se(4)	95.86(5)	Se(1)−P(1)−Se(3)	117.3(2)
Se(1)−Se(1′)−Se(6)	95.96(4)	Se(1)−P(1)−Se(4)	105.2(1)
Se(1)−Se(3′)−Se(2′)	72.27(5)	Se(5)−P(2)−Se(6)	107.6(1)
Se(1′)−Se(6)−Se(7′)	98.02(5)	Se(5)−P(2)−Se(7)	117.4(2)
Se(6)−Se(7′)−Se(2′)	74.24(5)	Se(5)−P(2)−P(2′)	105.9(3)

RE^{3+} centers are then coordinated by the highly charged $[P_ySe_z]^{n-}$ ligands. Good control of the Lewis basicity of the flux can be achieved by means of varying the starting composition.[5] In the case of **I**, **II** the basic flux was chosen to obtain compounds with the $[PSe_4]^{3-}$ unit (P^{5+}) (i.e. relatively high A_2-Se content). The successful synthesis of **I**, **II** validated this approach. For **III**, **IV** a relatively less basic flux was used to obtain predominantly the $[P_2Se_6]^{4-}$ unit (P^{4+}). Instead, **III**, **IV** possess both $[P_2Se_6]^{4-}$ and $[PSe_4]^{3-}$, indicating the presence a Lewis acid−base equilibria such as the one in eq 1.

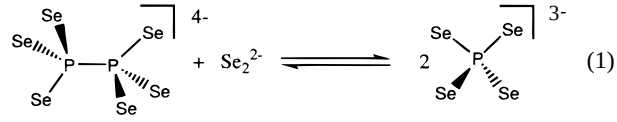

(1)

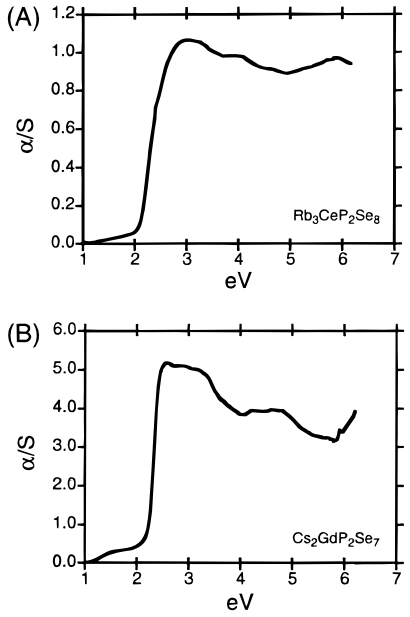

Figure 5. Solid-state optical absorption spectra of (A) $Rb_3CeP_2Se_8$ (**I**) and (B) $Cs_2GdP_2Se_7$ (**IV**).

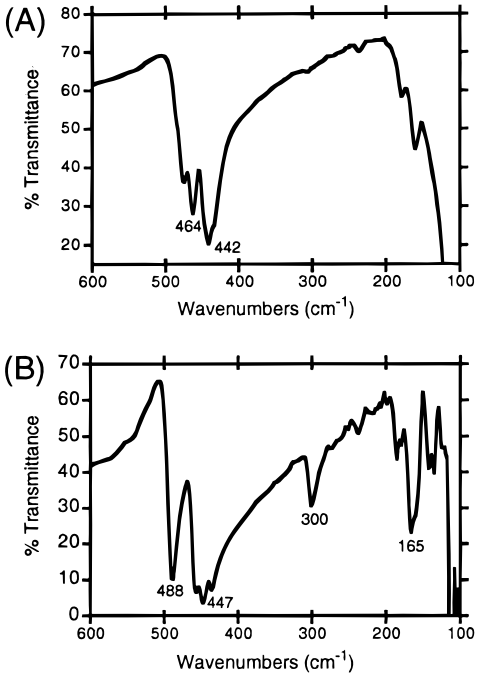

Figure 6. Far-IR spectra of (A) $Rb_3CeP_2Se_8$ (**I**) and (B) $Cs_2GdP_2Se_7$ (**IV**).

Table 6. Optical Band Gaps, Colors, Melting Points, and μ_{eff} Data

formula	E_g, eV	color	mp, °C	μ_{eff}, BM
$Rb_3CeP_2Se_8$	2.03	red	717	2.69
$Cs_3GdP_2Se_8$	2.21	orange	683	8.05
$Rb_2CeP_2Se_7$	2.00	red	808	2.43
$Cs_2GdP_2Se_7$	2.19	orange	747	7.96

All four compounds can be synthesized by direct elemental synthesis, indicating some thermodynamic stability of the products. This approach yields pure materials but in the form of microcrystalline powder. In addition to its exploratory value, the flux method produces good quality single crystals.

To place **I**−**IV** in a greater context, it is useful to consider them as members of a series with the general formula $(A_4P_2Se_6)_l(A_3PSe_4)_n[REPSe_4]_m$. The 3-D (RE)$PSe_4$ ($l = 0$, $n = 0$, $m = 1$) would be the parent member of the series. Interestingly, only the sulfur analogues (RE)PS_4 have been reported.[14,15] One can envision "dismantling" the network of the hypothetical (RE)PSe_4 by introducing one $[PSe_4]^{3-}$ unit per formula, to obtain the 1-D $A_3RE(PSe_4)_2$ ($l = 0$, $n = 1$, $m = 1$) (**I**, **II**), reported here. To maintain electroneutrality, of course, for every $[PSe_4]^{3-}$ unit that is introduced, three A^+ cations should follow. Addition of 2 more equivalents of A_3PSe_4 yields the molecular $A_9RE(PSe_4)_4$ ($l = 0$, $n = 3$, $m = 1$), which contains a mononuclear discrete complex.[6] The 2-D $A_4RE_2(PSe_4)_2(P_2Se_6)$ ($l = 1$, $n = 0$, $m = 2$) belongs to the same family and can be generated by introduction of 1 equiv of $A_4P_2Se_6$ to the parent (RE)PSe_4. This is illustrated in Scheme 1. Interestingly, when RE is divalent (e.g. Eu^{2+}) a similar family exists with the general formula $(A_3PSe_4)_n[RE_3(PSe_4)_2]_m$ and presently, the 2-D KEuPSe$_4$ ($n = 1$, $m = 1$)[2b] and the 1-D $K_4Eu(PSe_4)_2$ ($n = 4$, $m = 1$)[2a] have already been prepared.

Scheme 1

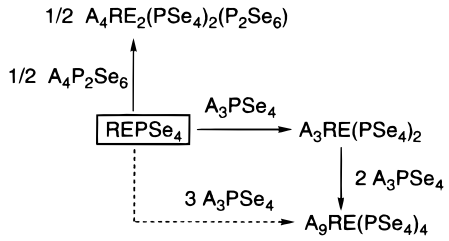

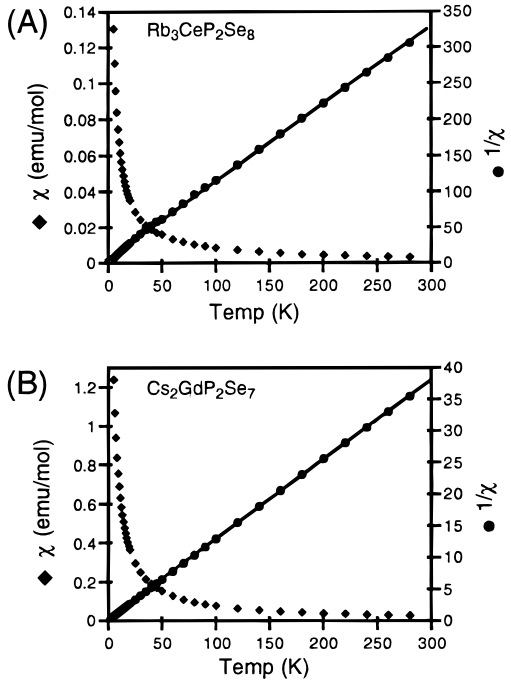

Figure 7. Plot of the molar magnetic susceptibility χ and $1/\chi$ vs temperature for (A) $Rb_3CeP_2Se_8$ (**I**) and (B) $Cs_2GdP_2Se_7$ (**IV**).

The solid-state UV/vis diffuse reflectance spectra of the compounds reveal sharp optical absorptions consistent with semiconductors, Figure 5. The estimated band gaps, E_g, are 2.03 eV for **I**, 2.21 eV for **II**, 2.00 eV for **III**, and 2.19 eV for **IV**. The values are identical, within the experimental error, for the Ce compounds **I** and **III** and for the Gd compounds **II** and **IV**.

(14) Rolland, B.; McMillan, P.; Molinié, P.; Colombet, P. *Eur. J. Solid State Inorg. Chem.* **1990**, *27*, 715.
(15) Wibbelmann, C.; Bronckner, W.; Eisenmann, B.; Schäfer, H. *Z. Naturforsch.* **1984**, *39a*, 190.

The far-IR spectra of **I**, **II** display absorptions at ca. 476, 464, and 442 cm^{-1} which can be assigned to $[PSe_4]^{3-}$ stretching modes but also two more absorptions at ca. 180 and 163 cm^{-1} assigned to RE−Se vibrations, Figure 6A.[2,3b,5,11] The infrared spectra of **III**, **IV** display absorptions at ca. 488, 457, 447, 435, 300, 237, and 227 cm^{-1}, Figure 6B. The ones at ca. 457, 300, 237, and 227 cm^{-1} are characteristic for the $[P_2Se_6]^{4-}$ group,[3a,5,7] whereas the rest are due to the $[PSe_4]^{3-}$. Absorptions at ca. 186, 165, 142, and 134 cm^{-1} are due to RE−Se vibrations.

DTA data followed by careful XRD analysis of the residues show that **I**−**IV** melt congruently in the 683−808 °C range, Table 6.

The magnetic susceptibility was measured as a function of temperature (5−300 K), Figure 7. All four compounds are paramagnetic, conforming to Curie law. The μ_{eff} values calculated from the slope of the straight line of the $1/\chi$ vs T data are 2.69, 8.05, 2.43, and 7.96 for **I**−**IV**, respectively. These values are consistent for Ce^{3+} (f^1) and Gd^{3+} (f^7) configurations.

The unusual low-dimensional structures of the compounds described here derive mainly from the highly elaborate coordination properties of the $[P_yQ_z]^{n-}$ groups. Control of flux composition and basicity is key in controlling which $[P_yQ_z]^{n-}$ ligands will appear in the compounds. It would be interesting to test if other putative members of the $(A_4P_2Se_6)_l(A_3PSe_4)_n$-$[(RE)PSe_4]_m$ family could be synthesized by direct synthesis using as a guide their predicted formula [for example the theoretical $A_6RE(PSe_4)_3$ ($l = 0$, $n = 2$, $m = 1$].

Acknowledgment. Financial support from the National Science Foundation Grant DMR-9527347 is gratefully acknowledged. M.G.K. is an A. P. Sloan Foundation and a Camille and Henry Dreyfus Teacher Scholar 1993−8. The authors are grateful to the X-ray Crystallographic Laboratory of the University of Minnesota and to Dr. Victor G. Young Jr. for collecting the single-crystal X-ray data set for $Rb_3CeP_2Se_8$. This work made use of the SEM facilities of the Center for Electron Optics at Michigan State University.

Supporting Information Available: Tables of crystallographic details for **I** and **IV**, anisotropic and isotropic thermal parameters of all atoms, interatomic distances and angles, and calculated and observed X-ray powder patterns for **I** and **IV** (35 pages). Ordering information is given on any current masthead page.

IC980025N